Correlated Roughness, Long-Range Correlations, and Dewetting of Thin Polymer Films

P. Müller-Buschbaum* and M. Stamm

Max-Planck-Institut für Polymerforschung, Ackermannweg 10, 55021 Mainz, Germany

Received October 9, 1997; Revised Manuscript Received March 9, 1998

ABSTRACT: The surface morphology of thin polymer films (polystyrene) on top of silicon substrates as prepared by spin-coating and after the dewetting of an initially homogeneous polymer film was examined. We investigated the influence of film thickness, molecular weight, annealing temperature, and used solvent. With diffuse X-ray scattering in the region of total external reflection a depth sensitivity was achieved. The in-plane structure of the untreated samples shows significant differences: Starting from a molecular weight of 28k the samples show conformal roughness over a range of film thickness between 50 and 1160 Å, whereas in an equivalent film thickness range for a low molecular weight sample no correlation between the substrate and the polymer surface was detected. Above the glass transition temperature the roughness correlation was lost and therefore has no influence on the dewetting behavior of the polymer films. A variation of the solvent used for the spin-coating gives rise to different dewetting structures that originate from different in-plane film structures right after the preparation. Thus, diffuse scattering is well suited for probing long-range correlations and mobility.

Introduction

New applications of polymers in electronics, biomedical, and nonlinear optics have stimulated an interest in thin films. In many of those applications, surface topography influences the optical, mechanical, thermal, or electrical characteristics. The wetting of a polymer film on a solid surface depends on the nature of long- and short-range interactions between the polymer and the solid.[1] In the case of complete wetting, a homogeneous wetting film results. Its thickness is controlled by the concentration used for the spin-coating.[2] With spin-coating, thin homogeneous polymer films may be prepared also on nonwetting surfaces. These films are metastable. Small perturbations lead to a relaxation toward the thermodynamical equilibrium.[3] In the picture of a spinodal dewetting process, fluctuations at the melt surface occur when heated above the glass transition temperature of the polymer. As a consequence, spontaneous dewetting results: The homogeneous film tears up and holes are formed. Holes grow in lateral size until a stable droplet formation is reached. The understanding of this dewetting process is currently a topic of great interest, displaying the limitations of any high-tech application, which requires a stable, homogeneous, and uniform film concerning thickness and density.

In recent experiments X-ray or neutron reflectivity measurements[4,5] and optical methods[6−9] have been used to investigate the different stages of the dewetting process. Less attention was paid to whether the preparation of the thin films via spin-coating itself has an influence on the dewetting studies. While polymer blends show surface structures right after the spin-coating[10−12] that result from the different volatility of the solvent,[12] homopolymer samples prepared by spin-coating exhibit smooth and featureless surfaces.[13,14] We performed diffuse X-ray scattering, which reveals the surface morphology. Additionally, due to the depth resolution, correlations between interfaces can be detected. We investigated the samples right after the preparation, in the melt and the final dewetting state. The influence of the annealing temperature, the film thickness, and molecular weight was examined. For polystyrene (PS) below the entanglement molecular weight M_e the polymer surface has no correlation with the substrate surface. Above M_e both interfaces are fully correlated, which means that the polymer film reproduces the substrate morphology. In the melt ($T > T_g$) this correlation vanishes and therefore can have no significant influence on the dewetting, which starts on a longer time scale. Additionally, no correlation between the drop structure of the dewetted film and the substrate was observed. Additionally, the influence of the used solvent during the spin-coating process was checked. This article has the following structure: The introduction is followed by an Experimental Section describing the sample preparation. The next section gives an introduction in diffuse scattering. Then the X-ray measurements are reported. Results and discussion conclude the paper.

Sample Preparation

We used native oxide covered Si(100) surfaces as obtained from the manufacturer (CrysTec Kristalltechnologie, Berlin) as substrates. Irrespective of the investigations concerning the influence of the used solvent, immediately before coating the dry wafers were washed in fresh toluene and the thin films were prepared by spin-coating (1950 rpm for 30 s) a toluene solution of the polymer onto the silicon substrate. For the solvent investigations toluene was replaced by cyclohexane (T = 40 °C) and THF. Polystyrene (PS) with several molecular weights M_w and a narrow molecular weight distribution M_w/M_n was used. Table 1 contains the polymers as well as the used abbreviations. Different film thicknesses were obtained by a variation in the concentration of the spin-coated solution following an empirical relation.[2]

Using X-ray reflectivity, the bare substrates were characterized and the initial film thicknesses of the polymer films were determined. All diffuse X-ray scattering experiments were performed in a vacuum sample

S0024-9297(97)01486-1 CCC: $15.00
Published on Web 05/08/1998

Table 1. Parameters of Polystyrene Materials Used: Molecular Weight M_w and Polydispersity M_w/M_n As Determined by GPC

abbreviation	M_w	M_w/M_n
PS9k	8 690	1.10
PS28k	28 000	1.05
PS31k	30 590	1.07
PS67k	66 630	1.08
PS106k	105 880	1.04
PS672k	672 000	1.05

cell with a thermoelectric heating. Due to the horizontally placed sample in-situ annealing of the samples was possible. Dewetting took place when the films were annealed in a vacuum furnace at 154 °C for different times. After the dewetting process reached a final state corresponding to a formation of isolated micrometer drops, the samples were quenched to room temperature and examined. An in-situ examination of the dewetting was not possible due to the very long annealing times (days).

Diffuse X-ray Scattering

As shown by Daillant and Bélorgey[15] off-specular scans yield direct information about the correlations between interfaces. The diffuse scattering cross section of an m-layer system was calculated by Holý and Baumbach[16] within the distorted-wave Born approximation (DWBA):

$$\left(\frac{d\sigma}{d\Omega}\right)_{diff} = \frac{F\pi^2}{\lambda^4}\sum_{j,k=1}^{m}(n_j^2 - n_{j+1}^2)(n_k^2 - n_{k+1}^2)^* \times \sum_{h,l=0}^{3} G_{h,j}G_{l,k}^* S_{j,k}^{h,l} \quad (1)$$

with

$$S_{j,k}^{h,l} = \exp\{-0.5[q_{h,j}^2\sigma_j^2 + q_{l,k}^{*2}\sigma_k^2] - i[q_{h,j}z_j + q_{l,k}^* z_k]\}(q_{h,j}q_{l,k}^*)^{-1} \times \int_0^\infty dX\,(\exp\{q_{h,j}q_{l,k}^* C_{j,k}(X)\} - 1)\cos(q_x X) \quad (2)$$

Note, that this expression automatically yields the kinematic result for large $|q_z\sigma|$.[17] The illuminated area of the sample is denoted by F, the refractive index of the jth layer is n_j, the rms roughness is σ_j, and the height−height autocorrelation function is $C_{j,j}(X)$. The Fourier transform of $C_{j,j}(X)$ is the power spectral density function (PSD) $L_{j,j}(q_x)$. The prefactors $G_{k,j}$ are defined as $G_{0,j} = T_{i,j}T_{f,j}$, $G_{1,j} = T_{i,j}R_{f,j}$, $G_{2,j} = R_{i,j}T_{f,j}$, and $G_{3,j} = R_{i,j}R_{f,j}$, with the amplitudes of the transmitted $T_{i,j}$, $T_{f,j}$ and the reflected waves $R_{i,j}$, $R_{f,j}$ within the jth layer. These amplitudes can easily be calculated using standard recurrence relations.[18−20] The z-component of the momentum transfer in each layer is given by $q_{0,j} = k_{(z,i),j} + k_{(z,f),j}$, $q_{1,j} = k_{(z,i),j} - k_{(z,f),j}$, $q_{2,j} = -q_{1,j}$, and $q_{3,j} = -q_{0,j}$, introducing the z-components $k_{(z,i),j}$ and $k_{(z,f),j}$ of the incident and diffracted wave vectors in medium j, respectively.

In a q_xq_z-map of the reciprocal space, the diffusely scattered intensity exhibits some characteristic features that are discussed in the following.

In a kinematic approximation of equation 1 structures caused by dynamic effects such as refraction are not visible. For a sample with uncorrelated interfaces all interfaces scatter independently and the diffuse intensities of all individual interfaces superpose. The case of partially or fully correlated roughness gives rise to scattering with partial coherence, the resonant diffuse scattering (RDS). The partial phase coherence of the waves diffusely scattered from different interfaces concentrates the intensity in narrow sheets. These sheets of resonant diffuse scattering are oriented parallel to the q_x-axis with the center fulfilling the one-dimensional Bragg condition[16]

$$\Delta q_z = \frac{2\pi}{d^{corr}} \quad (3)$$

The modulations of the resonant diffuse scattering are in phase with the fringes of the reflectivity and display the distance d^{corr} of the correlated interfaces. Due to the angle dependent refraction of X-rays the sheets are curved, forming the so-called "RDS bananas".[16]

One typical dynamical feature of diffuse scattering is the Yoneda peak.[21] It arises if the incident or exit angle equals the critical angle $\alpha_{i,f} = \alpha_c$. The intensity is enhanced because the standing wave field of the incident and reflected waves reached their maximum. So interference fringes can be additionally created by a waveguide behavior of two interfaces separated by a distance d^{dyn}. Higher orders $m_{i,f}$ of these dynamical originated fringes are damped out toward bigger q_z values. They occur independent of the actual interface correlation function if the modified Bragg condition[16]

$$2d^{dyn}\sqrt{n^2 - \cos^2(\alpha_{i,f})} = m_{i,f}\lambda \quad (4)$$

is fulfilled. The zeroth order is identical with the Yoneda peak.

In the case of a system consisting of one single layer on top of a semiinfinite substrate in a "detector scan", maxima due to roughness correlation and due to dynamical effects easily can be separated because they differ in their wavelength $\Delta\alpha_f^{corr}/\Delta\alpha_i^{dyn} \cong 2$. Therefore, one single detector scan is sufficient to give evidence for vertical replication of roughness.

X-ray Measurements

Because X-ray reflectivity delivers only information perpendicular to the surface,[18,19,21,22] a model assumption about the in-plane structure, based on other experimental techniques, frequently is applied.[4,23,24] This yields a laterally averaged density profile, which is used to fit the measured reflectivity curves. To obtain information about in-plane structures and correlation between interfaces, diffuse X-ray scattering has to be performed.[16,25,26]

X-ray reflectivity measurements of the homogeneous films directly after preparation without any further treatment as well as of these samples after dewetting were performed at a laboratory X-ray source.[27] The reflectivity curve of the homogeneous PS films exhibits well-pronounced fringes. This means that the film surface is very smooth with a surface roughness of typically 5 Å. A fit to the data yields film thicknesses of the PS9k and PS31k films of 50, 150, 400, 605, and 890 Å and of the PS28k films of 150, 220, 510, 990, and 1160 Å. The thickness of the thick PS28k film was estimated with an α-stepper (α-step 200, Tencor Instruments) to be 5000 Å. Dewetting essentially causes two changes in the laterally averaged density profile. The creation of holes reduces the mean density in the film

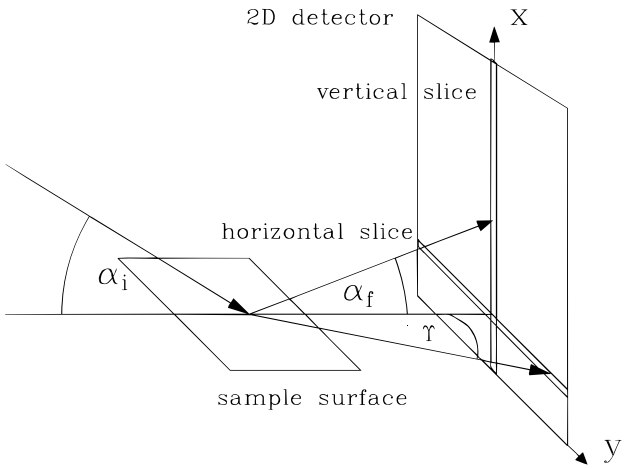

Figure 1. Schematic drawing of the experimental setup used in the X-ray experiment utilizing an 2D detector. The sample surface is horizontal. The angle of incidence is denoted with α_i, the exit angle with α_f and the out-of plane angle with Ψ. For data evaluation either vertical or horizontal slices can be taken.

region because polymer is replaced by air. The formation of the rim transfers material in a region above the once-prepared film and adds a tail to the density profile. Both effects lead to a smearing out of the density profile. A detailed model to describe the density profile of dewetted polymer films is presented in ref 4. Consequently, in the reflectivity curve of the dewetted sample as in the case of a big surface roughness no fringes are visible.

The diffuse X-ray measurements were performed at the BW4 USAX beamline of the DORIS III storage ring at HASYLAB/DESY in Hamburg. The selected wavelength was $\lambda = 1.55$ Å (and $\lambda = 1.77$ Å in an additional experiment). For further details concerning the beamline see ref 28. The instrument is normally used in transmission geometry. With the installation of a two-circle goniometer with a *z*-translation table, we employed a reflection geometry to realize diffuse X-ray scattering under the conditions of small-angle scattering with a setup of high-quality entrance slits and a completely evacuated pathway. The beam divergence in and out of the plane of reflection was set by two entrance cross slits. At an incident angle of $\alpha_i = 0.91°$ the coherently illuminated length on the sample surface is $\xi_{surf} \cong 500\ \mu$m, and perpendicular to the surface the coherence length is $\xi_{hor} \cong 8\ \mu$m.[29] The nonspecular as well as the specular intensity was recorded with a two-dimensional detector consisting of a 512 × 512 pixel array.[30] A sample−detector distance of 2917 mm (2843 mm) was chosen so that a resolution better than 1×10^{-3} Å^{-1} (9×10^{-4} Å^{-1}) was achieved. A beam-stop in front of the detector was installed at the position of the primary beam. At one fixed angle of incident α_i the two-dimensional intensity distribution consists of several vertical and horizontal slices. A schematic drawing is shown in Figure 1. As explained in ref 31, vertical slices correspond to detector scans and horizontal slices correspond to so-called "out-of-plane scans". The *xy*-plane denotes the sample surface and $\vec{q} = (q_x, q_y, q_z)$ the scattering vector.

In a common detector-scan the sample is held fixed at one angle of incidence α_i and the detector position is varied around the specular peak. According to $\Delta q_x \sim \pm(2\pi/\lambda)\alpha\Delta\alpha$ and $\Delta q_z \sim (2\pi/\lambda)\Delta\alpha$ the changes in the exit angle $\Delta\alpha$ will mainly result in a change of q_z and only very small changes in q_x. In a q_xq_z-map a detector scan is a parabolic path through the reciprocal space, which cuts the Yoneda as well as the specular streak. In a typical scan both peaks are visible. The intensity depends on the roughness of the sample and the chosen incident angle α_i. Additionally, in the case of correlated roughness one observes intensity streaks of a resonant diffuse scattering, which are oriented parallel to the q_x-axis. This yields a modulation of the intensity in a detector scan, as pointed out in the previous section.[32] Following eq 3 from the spacing of the fringes, one can estimate the distance between the correlated interfaces.

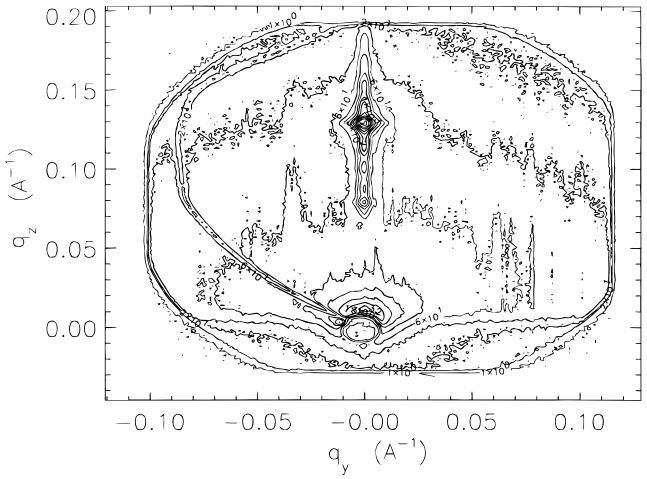

Figure 2. Contour plot of the scattered intensity distribution with a logarithmic contour line spacing. The primary beam, hidden under the beamstop, defines the position $q_y = q_z = 0$ Å^{-1}. The fixing of the beamstop with a thin wire causes a shadowing that leads to a reduced intensity in a region, which is without any further interest ($q_y < 0$ Å^{-1} and $q_z < 0.06$ Å^{-1}). The Yoneda peak is placed at $q_z = 0.08$ Å^{-1} and the specular peak at $q_z = 0.13$ Å^{-1}. Asymmetries in the background are caused by different efficiencies of the area detector and are corrected for the further data evaluation.

Results and Discussion

We performed measurements at an angle of incident $\alpha_i \gg \alpha_c$ above the critical angle of total reflection of the polymer film. Therefore, the typical characteristics of the scattered intensity (Yoneda peak, specular peak, modulations due to resonant diffuse scattering) can be easily separated. As an example, Figure 2 displays this for the PS28k sample. Because the off-specular scattering is several orders of magnitude below the specular intensity, the contour lines in Figure 2 are chosen with a logarithmic spacing. The most remarkably features of Figure 2 are the hidden primary beam (which defines $q_y = q_z = 0$ Å^{-1}), the Yoneda peak, and the specular peak. Additional peaks due to resonant diffuse scattering are visible, although in this presentation of the raw data the detector efficiency is not corrected.

Figures 3−6 show cuts along the direction of a detector scan where $\Phi = \alpha_i + \alpha_f$ denotes the detector angle. In the horizontal direction the intensity was integrated over $\Delta q_y = \pm 2.51 \times 10^{-3}$ Å^{-1}. The Yoneda peak is observed at $\Phi = 1.10°$ and the specular peak at $\Phi = 1.82°$. Additional modulations of the intensity originate from resonant diffuse scattering. In Figure 3 for one molecular weight of $M_w = 28\,000$ the thickness of the PS film is varied between 150 and 5000 Å. A comparison to the bare substrate (abbreviated with 0 Å) is shown, too. With the exception of the thick film,

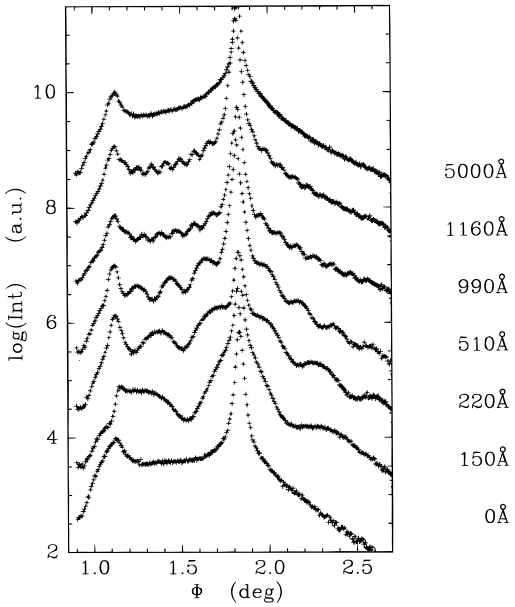

Figure 3. Detector scans measured at the angle of incidence $\alpha_i = 0.91°$ of the PS28k films as prepared for different film thicknesses. For clarity the curves are shifted by 1 order of magnitude against each other.

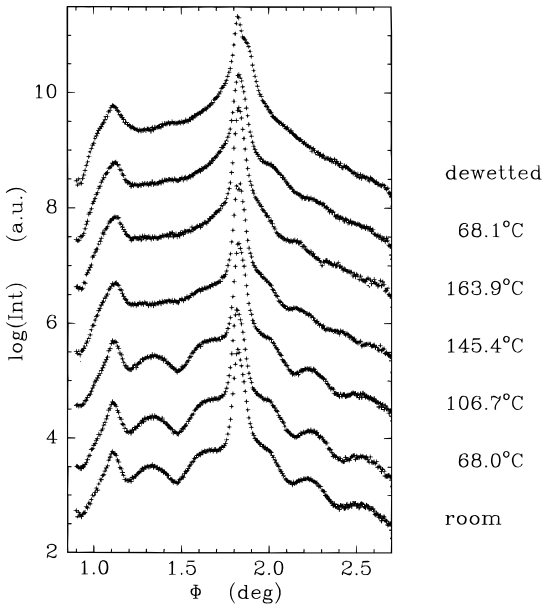

Figure 4. Detector scans measured at the angle of incidence $\alpha_i = 0.91°$ of the PS106k films with a film thicknesses $l = 220$ Å at different annealing temperatures (annealing time 15 min). For clarity the curves are shifted by 1 order of magnitude against each other.

all samples show correlated roughness. However, a roughness correlation over 5000 Å would lead to a spacing of the bragg sheets, which cannot be resolved in our experimental setup. Figure 4 pictures the influence of the annealing temperature for PS106k with a film thickness of 220 Å. After preparation the sample was heated in four different steps (68.0, 106.7, 145.4, and 163.9 °C) and cooled again in one step (68.1 °C). The annealing was performed at the corresponding temperature, staying 15 min at this temperature. The stability at the temperature was checked over 4 h (±0.5 deg). No dewetting was observed during the whole annealing cycle. When heated above the glass transition temperature T_g, in the melt state, the fringes in the detector scan vanish. After cooling, no reconstruction of the roughness correlation was observed, indicating an irreversible process. For a comparison the sample right after preparation (room) and after dewetting (dewetted) are presented, too. An equivalent behavior was found for other film thicknesses. The influence of the used solvent for the spin-coating is examined in Figure 5 with PS28k and a film thickness of 510 Å. Only the sample spin-coated from toluene solution shows conformal roughness. With both other solvents, THF and cyclohexane, no fringes are present. The molecular weight dependence at a fixed film thickness of 220 ± 20 Å is presented in Figure 6. Above the entanglement molecular weight M_e resonant diffuse scattering is detected, whereas below M_e the scattering curve exhibits no fringes. This behavior is proven over a big film thickness range with two additional sample series, as displayed in Figures 7 and 8. Figures 7 and 8 exhibit detector scans of PS9k and PS31k samples. In the left-sided graphs the intensity distribution measured from the samples as prepared and in the right-sided graphs the intensity distribution of the dewetted samples is displayed. The intensity has been integrated

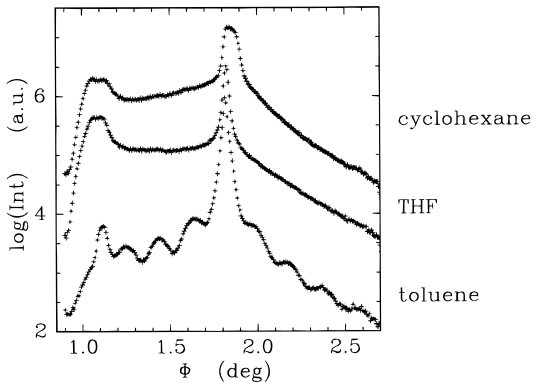

Figure 5. Detector scans measured at the angle of incidence $\alpha_i = 0.91°$ of the PS25k films with a film thicknesses $l = 510$ Å coated from solutions using different solvents. For clarity the curves are shifted by 1 order of magnitude against each other.

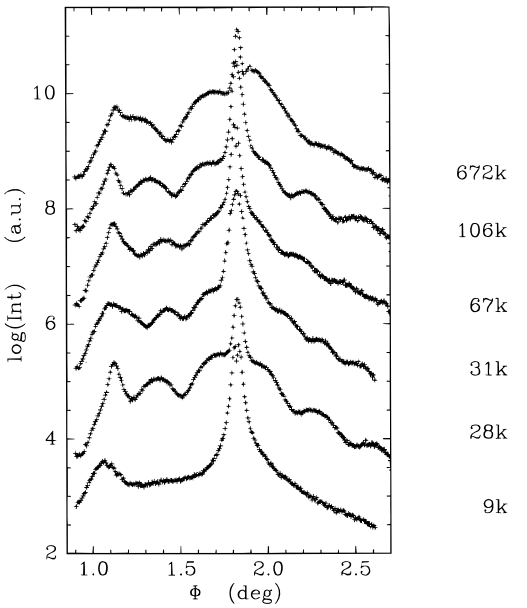

Figure 6. Detector scans measured at the angle of incidence $\alpha_i = 0.91°$ of films with a film thicknesses $l = 220 \pm 20$ Å at different molecular weights. For clarity the curves are shifted by 1 order of magnitude against each other.

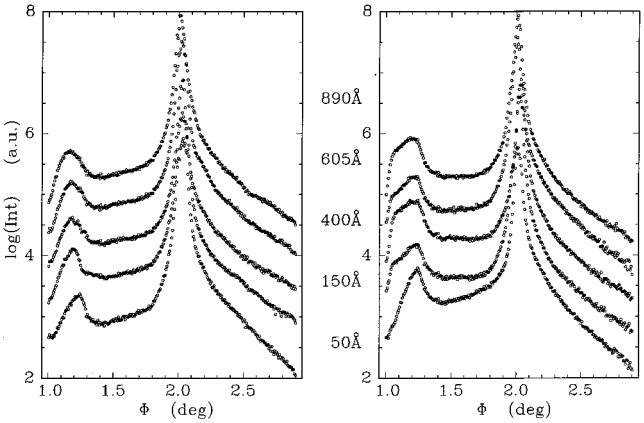

Figure 7. Detector scans measured at the angle of incidence $\alpha_i = 1.01°$ of the PS9k films as prepared (left side) and of the corresponding dewetted films (right side). From the bottom to the top the film thickness is in an equal range (50−890 Å) compared to the PS31k samples presented in Figure 8. For clarity the curves are shifted by 1 order of magnitude against each other.

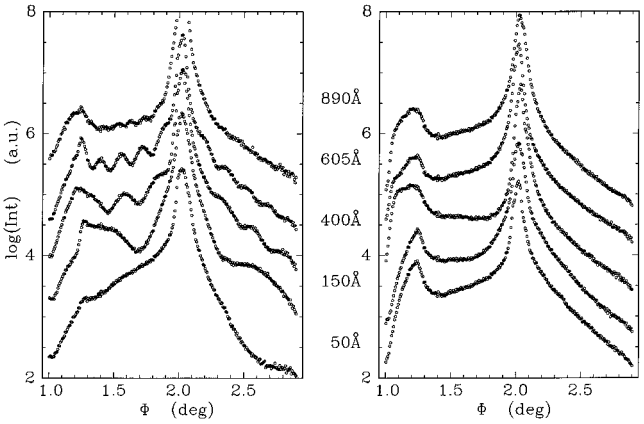

Figure 8. Detector scans measured at the angle of incidence $\alpha_i = 1.01°$ of the PS31k films as prepared (left side) and of the corresponding dewetted films (right side). From the bottom to the top the film thicknesses are 50, 150, 400, 605, and 890 Å. For clarity the curves are shifted by 1 order of magnitude against each other.

in a horizontal direction from $\Delta q_y = \pm 2.25 \times 10^{-3}$ Å^{-1}. The Yoneda peak is observed at $\Phi = 1.20°$ and the specular peak at $\Phi = 2.02°$. In the case of the PS9k samples (Figure 7) the scattering curves show no modulations originating from conformal roughness. Only the Yoneda and the specular peaks are visible. Changes in the scattered intensities between the homogeneous and the dewetted films are observable in an extension of the Yoneda peak toward smaller angles Φ. This corresponds to a decrease of the mean density and an increase in surface roughness of the PS film due to the formation of drops, as explained above in the description of the calculation of the density profile. In the case of the PS31k samples the behavior is remarkably different: The intensity distribution right after preparation is dominated by well-pronounced fringes (left side of Figure 8). Again they result from conformal roughness. The wavelength of the fringes depends on the spacing between both correlated interfaces. From the resulting values, which correspond to the whole film thickness of the 31k PS film, we can conclude that the correlation concerns the polymer−air and the substrate−polymer interface. In the curves of the dewetted samples no fringes are present and the dewetting structure seems not to be correlated to the substrate roughness.

The spin-coating process consists of several stages: First a polymer solution at low concentration is dropped onto the substrate, which then is started to spin. During the initial stages most of the solution is centrifuged off, leaving a thin layer on the substrate. As the layer thins due to fluid flow, the evaporation of the solvent becomes important. The evaporation increases the viscosity of the polymer solution and slows the shear thinning of the film. Solvent evaporation freezes in the developing surface structure generally in a nonequilibrium stage, as demonstrated for a thin blend film of PMMA/PS.[12] A correlation between two interfaces yields a dependence of the in-plane morphology of the upper layer from the underlying one. In a one-layer system the film follows the curvature of the substrate like a thin layer of snow, if both are fully correlated (hill is on top of a hill and a valley on top of a valley). In multilayer systems the number of correlated interfaces increases, which is frequently examined in thin solid films,[32−37] Langmuir−Blodgett films,[38] or smectic films.[39]

Influence of Film Thickness. Roughness correlation was observed over a big film thickness range, which includes thicknesses corresponding to several times the radius of gyration R_g (e.g., PS28k $R_g = 45$ Å, compare Figure 3). Thus we observe a collective phenomena of many chains. In the framework of a linear response theory the roughness correlation of thin films is described by Andelmann et al.[40] Long wavelength fluctuations of the solid surface are followed by the liquid interface and short wavelength fluctuations are damped out by surface tension. With increasing film thickness the liquid interface becomes smoother and undulations of the solid surface are followed more closely as the film thickness decreases. Experimentally, this effect was confirmed for thin polymer films on top of surface gratings[41,42] that were used as substrates with a roughness dominated by one Fourier component. But the description by Andelmann implies thermodynamical equilibrium and is therefore not applicable for our investigation. Thin polymer films as prepared and stored below the glass transition temperature are far away from equilibrium. Therefore, the surface is dominated by effects of the spin-coating process, which is only hardly investigated, mostly in the case of polymer blends,[10−12] depending on the storage time after the preparation due to kinetic effects. Far below T_g kinetics are significantly suppressed and the morphology induced by the spin-coating is frozen in.

Influence of Annealing. Polymer chains can be regarded as immobile below T_g. Thus, annealing at temperatures below T_g (e.g., $T = 68.0$ °C in Figure 4) does not remove the roughness correlation. Above T_g the thin polymer film is in a melt state and polymer chains get mobile. Near a free surface, the mobility of lower molecular weight polymers is increased over that in the bulk, but higher molecular weight polymers exhibit no change in mobility.[43] From the annealing study shown in Figure 4 it can be concluded that near T_g at $T = 106.7$ °C the chain mobility is very low because after 4 h still the interface correlation is present. At $T = 145.4$ °C the mobilitiy is sufficiently enlarged to remove the roughness correlation and a main contribution to the surface roughness σ is due to thermal fluctuations at the liquid surface. A further increase in annealing temperature increases this contribution to

the surface roughness $\sigma \sim T/\gamma_{LV}$.[44] The surface tension is denoted with γ_{LV}. Quenching down the sample to a temperature well below T_g freezes in this present surface structure. Therefore in Figure 4 the scattered intensities at $T = 163.9$ °C and $T = 68.1$ °C look quite similar.

Influence of Molecular Weight. In the case of PS9k T_g decreased by roughly 10 K compared to PS31k.[45] Additionally, the molecular weight 9k is below the entanglement molecular weight $M_e = 18\ 100$[46] and the polymer melt behaves more like a liquid than like a entangled polymer. The motion of the chain is unrestrained and the chain diffuses in a Rouse-like manner. Entanglements restrict the mobility of the molecules in the bulk and in concentrated solutions, as they occur due the evaporation of the solvent during the spin-coating. They are the basis of many of the unique and unusual dynamic properties of polymers. Qualitatively, an entanglement can be envisioned as a crossing of polymer chains, which remains intact and hence mechanically active, when subjected to a strain. One has to keep in mind, however, that structures forming during solvent evaporation and viscosity also depend strongly on molecular weight.

Independent of the initial film thickness in a range between 50 and 890 Å, PS films with a molecular weight below 28k have a surface that shows no correlation with the underlying substrate. Above this molecular weight both interfaces are strongly correlated. Heated above the glass transition temperature these correlations vanish. This does not imply that the films have reached their equilibrium; however, the state of the homogeneous but uncorrelated polymer film stays metastable until dewetting sets in. The same behavior was observed for even higher molecular weights than 31k. The time scale of this loss in correlation is significantly smaller than the time scale of the dewetting of the polymer film. In the framework of spinodal decomposition as an origin of the dewetting the time constant scales with l[5,47,48] and is enlarged with higher molecular weights. After a final dewetting state characterized by the formation of mesoscopic drops is reached, the surface structures of both sample systems, low and high M_w, are comparable. Therefore, the dewetting is independent of the initial surface morphology, which results from the spin-coating process using one fixed solvent.

Influence of Used Solvent. Using solvents other than the frequently applied toluene leads to thin films that have a surface in-plane structure right after the spin-coating and show a different dewetting behavior. In Figure 9a−f optical micrographs are presented. On the left-hand side the surface morphology of the prepared film (magnification 4 times) and on the right-hand side that of the dewetted film (magnification 10 times) are displayed. The films spin-coated from a cyclohexane solution have a radial structure picturing the material flow during the rotation of the sample. Due to the high evaporation rate of THF during the spin-coating the surfaces of the corresponding films look inhomogeneous, too. Both samples exhibit no conformal roughness and thus the morphology of the polymer surface is not influenced by the substrate morphology. Different dynamics of the solvent removal and different contact angles between solvent and substrate dominate the resulting thin film. As a consequence, the dewetting behavior differs. Whereas the samples spin-coated from toluene solution exhibit the well-known[6−9] drop pattern

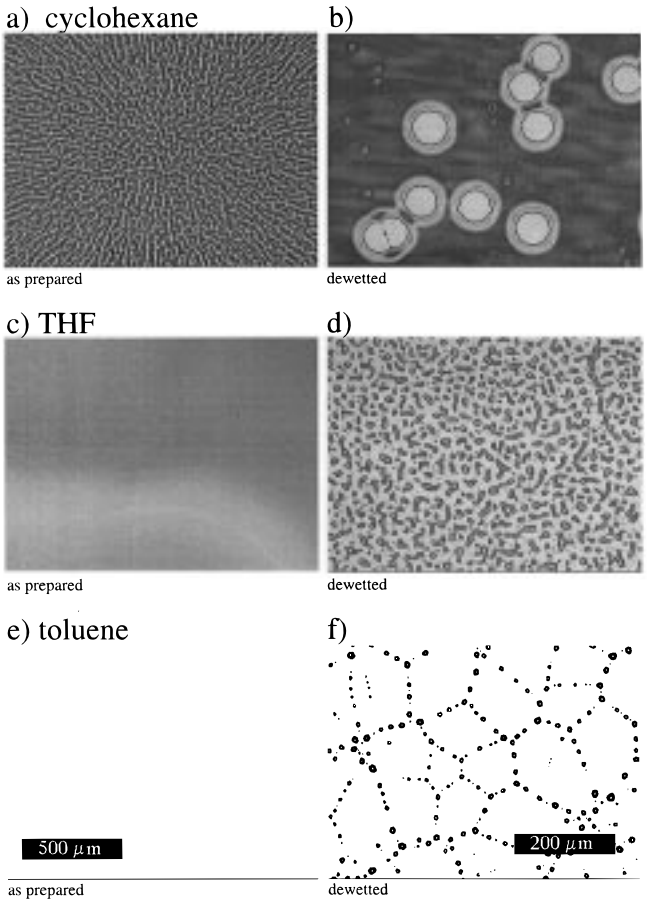

Figure 9. Optical micrographs of PS28k samples coated from solutions that differ in the solvent right after preparation (left side, magnification 4 times) and dewetted in a vacuum furnace (right side, magnification 10 times).

with hexagonal arrangement (Figure 9f) with changed solvent another drop structure results (Figure 9b,d). Therefore, this structural information imposed by the thin film formation dominates the further dewetting structure.

In summary, two different types of in-plane morphologies induced during the spin-coating process are observed, which differ in their influence on the dewetting of thin polymer films. Whereas roughness correlations are lost on a shorter time scale than dewetting, surface structures originated by different solvent dynamics dominate further dewetting. Investigating the relaxation of conformal roughness before the onset of dewetting probes the mobility of polymer chains in thin film geometry. Therefore, real time experiments with an increased time resolution might display the evolving spectral power density function of the polymer surface and give new insights into the formation of capillary waves. Additionally, the determination of surface diffusion coefficients will be possible.

Acknowledgment. We want to thank T. Kuhlmann, J. Kraus, C. Lorenz, and A. Vix for their help during the X-ray measurement. Additionally, we owe many thanks to S. Cunis, G. von Krosigk, and U. Lode for the technical assistance at the BW4 beamline, as well as to R. Gehrke for his general support of the experiment at HASYLAB. This work was supported within the European Community program HCM-ERBCHBICT941717 and C11-CT-93-0351 as well as by DFG.

References and Notes

(1) Israelachvili, J. N. *Intermolecular and surface forces*, 2nd ed; Academic Press: London, 1991.
(2) Schubert, D. W. *Polym. Bull.* **1997**, *38*, 177.
(3) Dietrich, S. In *Phase Transitions and Critical Phenomena*; Domb, C., Lebowitz, J. L., Eds.; Academic: New York, 1988; Vol. 12.
(4) Reiter, G. *Macromolecules* **1994**, *27*, 3046.
(5) Reiter, G.; Auroy, P.; Auvray, L. *Macromolecules* **1996**, *29*, 2150.
(6) Redon, C.; Brochard-Wyart, F.; Rondelez, F. *Phys. Rev. Lett.* **1991**, *66*, 715.
(7) Reiter, G. *Phys. Rev. Lett.* **1992**, *68*, 75.
(8) Reiter, G. *Langmuir* **1993**, *9*, 1344.
(9) Redon, C.; Brzoska, J. B.; Brochard-Wyart, F. *Macromolecules* **1994**, *27*, 468.
(10) Affrossman, S.; Henn, G.; O'Neill, S. A.; Pethrick, R. A.; Stamm, M. *Macromolecules* **1996**, *29*, 5010.
(11) Jandt, K. D.; Heier, J.; Bates, F. S.; Kramer, E. J. *Langmuir* **1996**, *12*, 3716.
(12) Kumacheva, E.; Li, L.; Winnik, M. A.; Shinozaki, D. M.; Cheng, P. C. *Langmuir* **1997**, *13*, 2483.
(13) Weil, A. In *The Physics and Fabrication of Microstructures and Microdevices*; Kelly, M. J., Weisbruch, C., Eds.; Springer-Verlag: Berlin, 1986; p 51.
(14) Jenekhe, S. A. In *Polymers for High Technology*; Bowden, M. J., Turner, S. R., Eds.; ACS Symposium Series: Washington, DC, 1987; Vol. 346.
(15) Daillant, J.; Bélorgey, O. *J. Chem. Phys.* **1992**, *97*, 5824.
(16) Holý, V.; Baumbach, T. *Phys. Rev. B* **1994**, *49*, 10668.
(17) Sanyal, M. K.; Sinha, S. K.; Gibaud, A.; Satija, S. K.; Majkrzak, C. F.; Homa, H. *Springer Proc. Phys.* **1992**, *61*, 91.
(18) Born, M.; Wolf, E. In *Principles of Optics*; Pergamon Press: Oxford, U.K., 1964.
(19) James, R. W. In *The Optical Principles of the Diffraction of X-rays*; OxBow Press: Woodbridge, CT, 1962.
(20) Lekner, J. In *Theory of Reflection*; Martinus Nijhoff Publishers: Dodrecht, The Netherlands, 1987.
(21) Yoneda, Y. *Phys. Rev.* **1963**, *131*, 2010.
(22) Parrat, L. G. *Phys. Rev.* **1954**, *55*, 359.
(23) Müller-Buschbaum, P.; Tolan, M.; Press, W.; Brinkop, F.; Kotthaus, J. P. *Ber. Bunsen-Ges. Phys. Chem.* **1994**, *98*, 413.
(24) Henn, G.; Stamm, M.; Poths, H.; Rücker, M.; Rabe, J. P. *Physica B* **1996**, *221*, 174.
(25) Sinha, S. K.; Sirota, E. B.; Garoff, S.; Stanley, H. B. *Phys. Rev. B* **1988**, *38*, 2297.
(26) Pynn, R. *Phys. Rev. B* **1992**, *45*, 602.
(27) Foster, M.; Stamm, M.; Reiter, G.; Hüttenbach, S. *Vacuum* **1990**, *41*, 1441.
(28) Gehrke, R. *Rev. Sci. Instrum.* **1992**, *63*, 455.
(29) Salditt, T.; Rhan, H.; Metzger, T. H.; Peisl, J.; Schuster, R.; Kotthaus, J. P. *Z. Phys. B* **1995**, *96*, 227.
(30) Müller-Buschbaum, P.; Vanhoorne, P.; Scheumann, V.; Stamm, M. *Europhys. Lett.* **1997**, *40*, 655.
(31) Salditt, T.; Metzger, T. H.; Peisl, J.; Goerigk, G. *J. Phys. D: Appl. Phys.* **1995**, *28*, A236.
(32) Stettner, J.; Schwalowsky, L.; Seeck, O. H.; Tolan, M.; Press, W.; Schwarz, C.; Känel, H. v. *Phys. Rev. B* **1996**, *53*, 1398.
(33) Stearns, D. G. *J. Appl. Phys.* **1992**, *9*, 4286.
(34) Fullerton, E. E.; Pearson, J.; Sowers, J. H.; Bader, S. D.; Wu, X. Z.; Sinha, S. K. *Phys. Rev. B* **1993**, *48*, 17432.
(35) Baumbach, G. T.; Holý, V.; Pietsch, U.; Gailhanou, M. *Physica B* **1994**, *198*, 249.
(36) Schlomka, J. P.; Tolan, M.; Schwalowsky, L.; Seeck, O. H.; Stettner, J.; Press, W. *Phys. Rev. B* **1995**, *51*, 2311.
(37) Kaganer, V. M.; Stepanov, S. A.; Köhler, R. *Physica B* **1996**, *221*, 34.
(38) Nitz, V.; Tolan, M.; Schlomka, J. P.; Seeck, O. H.; Stettner, J.; Press, W.; Stelzle, M.; Sackmann, E. *Phys. Rev. B* **1996**, *54*, 5038.
(39) Mol, E. A.; Shindler, J. D.; Shalaginov, A. N.; de Jeu, H. W. *Phys. Rev. B* **1996**, *54*, 536.
(40) Andelmann, D.; Joanny, J. F.; Robbins, M. O. *Europhys. Lett.* **1988**, *7*, 731.
(41) Tolan, M.; Vacca, G.; Sinha, S. K.; Li, Z.; Rafailovich, M.; Sokolov, J.; Lorenz, H.; Kotthaus, J. P. *J. Phys. D: Appl. Phys.* **1995**, *28*, A231.
(42) Tolan, M.; Vacca, G.; Wang, J.; Sinha, S. K.; Li, Z.; Rafailovich, M.; Sokolov, J.; Gibaud, A.; Lorenz, H.; Kotthaus, J. P. *Physica B* **1996**, *221*, 53.
(43) Tanaka, K.; Taura, A.; Ge, S.; Takahara, A.; Kajiyama, T. *Macromolecules* **1996**, *29*, 3040.
(44) Braslau, A.; Pershan, P. S.; Swislow, G.; Ocko, B. M.; Als-Nielsen, J. *Phys. Rev. A* **1988**, *38*, 2457.
(45) Brandrup, J.; Immergut, E. H. In *Polymer Handbook*, 3rd ed.; John Wiley & Sons: New York, 1989.
(46) Ferry, J. D. In *Viscoelastic properties of polymers*; John Wiley & Sons: New York, 1980.
(47) Brochard-Wyart, F.; Redon, C.; Sykes, C. *C. R. Acad. Sci. Ser. 2* **1992**, *19*, 314.
(48) Yerushalmi-Rozen, R.; Klein, J. *Langmuir* **1995**, *11*, 2806.

MA971486F